A Numerical Study on Active Control for Tiltrotor Whirl Flutter Stability Augmentation

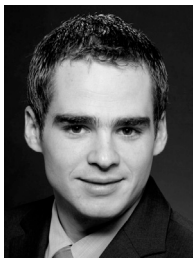

Joerg P. Mueller*
Dynamics Engineer
Eurocopter
Marignane, France

Yves Gourinat
Professor
SUPAERO
Toulouse, France

Rogelio Ferrer
Dynamics Engineer
Eurocopter
Marignane, France

Tomasz Krysinski
Dynamics Manager
Eurocopter
Marignane, France

Benjamin Kerdreux
Dynamics Engineer
Eurocopter
Marignane, France

ABSTRACT

The use of active control to augment whirl flutter stability of tiltrotor aircraft is studied by means of a multibody simulation. The numerical model is based on a 1/5 scale semi-span aeroelastic wind tunnel model of a generic tiltrotor concept and possesses a gimballed, stiff-in-plane rotor that is windmilling. A single-input single-output controller and two types of multi-input multi-output algorithms, Linear Quadratic Gaussian Control and Generalized Predictive Control, are studied. They are using measured wing deflections in order to calculate appropriate swashplate input. Results on the closed-loop behavior of three wing and two gimbal natural modes are given. Robustness analyses with respect to major parameters like wing natural frequencies or structural damping are also briefly discussed. The rotor shear force is shown in the uncontrolled condition and in presence of a controller in order to illustrate the whirl flutter mechanism. The single-input single-output controller yielded substantial gain in stability and turned out to be most suitable for industrial application, whereas the Linear Quadratic Gaussian Regulator yielded even higher damping and still had good robustness characteristics.

NOTATION

f	frequency
g	controller gain
h	flight altitude
m	number of plant inputs
p	model order
q	natural mode
r	number of plant outputs
u	plant input
w_r	weight on command angles (GPC)
x	state vector
$\hat{x}$	estimator state vector
y	plant output
G	plant transfer function
H	controller transfer function
J	performance index
K	controller gain matrix

* Currently: Aeroelastics Engineer, AIRBUS, Bremen, Germany

Revised version of the paper "A Multibody Study on Single- and Multi-Variable Control Algorithms for Tiltrotor Whirl Flutter Stability Augmentation", presented at the American Helicopter Society 4th Decennial Specialist's Conference on Aeromechanics, Fisherman's Wharf, San Francisco, California, January 21-23, 2004.

β_+ rotor progressive gimbal flap mode
β_- rotor regressive gimbal flap mode
ζ damping, % critical
θ_{1c} longitudinal cyclic swashplate input
θ_{1s} lateral cyclic swashplate input
θ_0 collective swashplate input
advance ratio, forward speed / blade tip speed
ρ parameter governing state estimator dynamics (LQG)
ϕ phase angle
φ wing degree of freedom (deflection angle)
ω angular velocity
Ω rotor rotation speed

Subscripts

$()_b$ value related to wing beamwise bending
$()_c$ value related to wing chordwise bending
$()_d$ all pass
$()_G$ plant related
$()_H$ controller related
$()_{hp}$ high pass
$()_{lp}$ low pass
$()_t$ value related to wing torsion
$()_{crit}$ critical quantity (flutter point)

INTRODUCTION

Tiltrotor aircraft have been the subject of research and development since well before the 1950's when the first flight of the *Transcendental 1G* took place. Considerable experience in tiltrotor design was acquired with the research aircraft *XV-3* and *XV-15* that followed, but the first tiltrotor to enter service in the near future will be the military *V-22 Osprey* and the smaller *BA-609* for the civil and parapublic market. The most recent European tiltrotor concept *ERICA* is presented in Fig. 1. Tiltrotor aircraft provides unique features as it combines the advantages of helicopters, notably vertical take off, landing and hover capabilities, with the high cruise speed and range of turboprop airplanes.

The tiltrotor concept is subject to an instability called *whirl flutter*, which occurs in high speed flight in the airplane configuration, and which constitutes an important factor in tiltrotor design as it can lead to very high dynamic loads. It is therefore necessary to guarantee adequate stability margins throughout the flight envelope.

Studies into aeroelastic stability augmentation focus basically on the design of more efficient aircraft. A second objective is to extend stability boundaries with respect to flight speed. One major structural design parameter influencing whirl flutter stability is the wing (torsional-) stiffness. For this reason, today's tiltrotor concepts have wing structures with a high thickness to chord ratio, typically 21 % to 23 %, inducing high aerodynamic drag in cruise. Therefore, it would be advantageous to provide adequate stability by other means in order to reduce wing stiffness requirements.

Whirl flutter on tiltrotor aircraft was discovered during fullscale wind tunnel testing of the XV-3 research aircraft in the early 1960's. On an articulated rotor, the destabilizing effect is generated by large in-plane forces that act on the pylon. They become destabilizing in the high-inflow condition and are the direct result of cyclic blade incidence variations that arise during nacelle pitch and yaw motion as the rotor tip path plane is following the plane perpendicular to the rotor mast with a time lag, Ref. 1. Consequently, the phenomenon can occur in a combined manner on the pitch and yaw axes but also on one axis only. Furthermore, forward and retrograde whirl is possible.

In the past, considerable work has been done on passive optimization of wings and rotors. The influence of different design parameters, like wing frequencies, wing sweep or rotor flap and lag dynamics, is presented in Ref. 2. Formal optimization techniques with the objective to find an optimal set of rotor design parameters are reported in Ref. 3 where the main parameters considered are pitch-flap and pitch-lag couplings, blade flapping flexibility distribution and wing stiffness.

Active control has been studied with the objective of expanding the tiltrotor flight envelope and enhance maneuverability, versatility and ride qualities. In this context, the aspects of gust response and maneuver loads with respect to rotor loads, drive train loads and vibration behavior have been looked at in Refs. 4 and 5. On the other hand, less work has been done on active control for aeroelastic stability augmentation. The aim of the latter is to enable the aircraft to fly at higher speeds, to descend more steeply or to reduce structural stiffness and therefore weight. The advent of fly-by-wire control systems with powerful flight control computers has made feasible the implementation of controllers of higher complexity for stability augmentation. Recent actuator technology is able to handle commands of required bandwidth, and the controller commands can therefore be applied directly on the control system.

The potential of aeroelastic control to increase dynamic stability margins has been studied in Refs. 6 to 12. The first three references deal with rather direct feedback to the

Fig. 1. Artist's illustration of the European ERICA advanced tiltrotor concept.

swashplate. Either wing deformation (Ref. 6) or velocity and acceleration measurements (Refs. 7, 8) are used for feedback. As these control laws are basically single-input single-output (*SISO*) or a combination of several SISO channels, their effectiveness on multiple natural modes is limited. In order to increase stability in a more comprehensive manner, multi-input multi-output (*MIMO*) algorithms have also been studied. In Ref. 9, a *Linear Quadratic Regulator* with a state estimator is presented that is based on analytical equations of the tiltrotor dynamics. In modal space, stable and unstable modes were separated and the controller was designed for the unstable modes only. A more recent MIMO control theory, the *Generalized Predictive Control*, was evaluated in Ref. 4 for maneuver load alleviation using a multibody model and in Ref. 11 for flutter control using wind tunnel tests.

As a complement to the cited publications, the present paper evaluates a SISO controller and two MIMO control algorithms by means of the same numerical modeling approach. Thus, a direct comparison of different control strategies is possible. The SISO controller is based on a 180° out-of-phase feedback of wing motion to the swashplate whereas Linear Quadratic Gaussian Control and Generalized Predictive Control were chosen for MIMO studies. A general purpose multibody analysis tool is used as the central simulation engine.

Frequency and damping of three fundamental wing modes and two rotor flap modes are presented up to the closed-loop stability boundaries. A comparison of the robustness of the control algorithms with respect to variations in wing natural frequencies, structural damping, flight speed, rotation speed, flight altitude, and signal noise are presented. The work is done with the objective of developing the methods and knowledge for application to subsequent wind tunnel tests. Thus, system identification techniques have been applied to describe the dynamics of the rotor system. Physical illustration of controller action is given by comparing the controller generated rotor shear forces with the oscillation to be attenuated.

The paper is organized as follows: In the next section, the numerical model and a brief validation are described. The basic equations underlying the control algorithms are described thereafter, together with a description of the identification techniques that are used to determine the system transfer functions from swashplate input to wing deflection. The subsequent section summarizes the basic procedure of the numerical simulation and the analysis techniques that are generally applied in the time domain. The determination of identification and controller parameters is also presented in detail. A results section presents an evaluation of the three control techniques, and the paper closes with the conclusions and gives recommendations about the most suitable algorithms.

NUMERICAL MODEL

Model Configuration

For this initial investigation, a semi-span proprotor model with a cantilevered wing is chosen and the portside rotor is modeled. This configuration contains the basic features of tiltrotor dynamics and has been the subject of much theoretical and experimental work. A windmilling rotor has been chosen, as it was found in past research that this is a conservative approach. Due to this assumption, the dynamic model is further simplified as the drive-train and the engine dynamics are less important. This is favorable for system identification and controller design and reduces the complexity of the numerical model, which means substantial advantages in terms of computation speed and numerical stability.

The main degrees of freedom are three wing deflections and the two gimbal flapping angles. The corresponding fundamental wing natural modes beamwise bending, chordwise bending, and torsion are modeled as they contribute to the principal mechanism involved in whirl flutter. Cyclic flapping of the rotor is accounted for by the gimbal joint. Other rotor flexibility is not included, even though rotor coning as well as collective and cyclic lag dynamics do have some influence on whirl flutter (Ref. 13). These choices were made in the context of the development of control algorithms where it is important to keep the system order rather low. This allows focusing on the critical modes and therefore designing an efficient controller tailored to those modes.

The baseline for this work is a generic tiltrotor design inspired by the new European *ERICA* concept (Ref. 14). Its dynamic characteristics have been translated to a 1/5 scale aeroelastic model using Froude scaling as summarized in Table 1. Here, the rotor blade inertias and static moments are given with respect to the hub center. Contrarily to the ERICA rotor, an equivalent three-bladed rotor is modeled in order to be as close as possible to an in-house wind tunnel model. This equivalence has been achieved by keeping a similar Lock number and solidity for the three-bladed rotor as the four-bladed rotor model would have. The aerodynamic coefficients are approximations taken from airfoil data. Flapping inertia of hub and control system as well as control system mass are neglected. Furthermore, no spring stiffness in the gimbal joint is taken into account. Finally, the nacelle containing engine and gear box is assumed to be rigidly attached to the wing, the wing itself being modeled as one entity in terms of mass and inertia.

For modeling the principal aerodynamic forces, a simple blade element model has been used. No inflow model has been considered as the rotor induced flow field is less important in the high-inflow condition. Furthermore, incompressible airfoil characteristics have been used that are justified by the low velocity at the blade tip of well bellow Mach 0.3 even in forward flight. Wing aerodynamics are not taken into account since previous investigations showed that it has

Tabel 1. Model data.

Parameter	Symbol	Value
Rotor		
radius	R	729 mm
number of blades	b	3
solidity (thrust wtd.)	σ	0.18
rotation speed	n_r	950 $^{\text{rev}}/_{\text{min}}$
distance of rotor center from conversion axis		331 mm
mass	m_b	0.51 kg
blade static moment	m_s	0.2 kg m
blade flapping inertia	I_β	0.081 kg m^2
Lock number	γ	3.4
twist (non-lin. distrib.)	θ_t	$-35\,^\circ$
lift coefficient ($\alpha = 0$)	$c_{l,0}$	0.34
lift curve slope	$c_{l,\alpha}$	5.7 rad^{-1}
drag coefficient ($\alpha = 0$)	$c_{d,0}$	$7.5 \cdot 10^{-3}$
quadratic drag coeff.	$c_{d,\alpha}$	0.8 rad^{-2}
Pitch control system		
pitch-flap coupling	δ_3	$-20\,^\circ$
Hub and const. vel. joint		
mass	m_{hub}	1.07 kg
Wing		
half wingspan		1480 mm
equivalent beam length		980 mm
mass	m_w	3.22 kg
structural damping	ζ_s	3 %
Nacelle		
mass	m_n	6.62 kg

a slightly stabilizing effect. The rotation axis is assumed to be parallel to the forward speed vector of the aircraft.

A numerical simulation model based on this data was built using a general purpose multibody simulation tool with multiple interfaces to industrial design tools and control software. The numerical model generation is partially based on a CAD virtual mockup of the wind tunnel model for geometry and mass data, which highlights the benefits of integrating the dynamic simulation within the virtual prototyping framework. After extraction of the main bodies, the articulations have to be added and rotor blade aerodynamics have to be implemented in the model by explicit formulation of force vectors. The industrial multibody code, being not specially adapted to rotating systems and periodicity, provides no direct stability analysis and linearization mechanisms. Thus, the stability characteristics have been extracted from time domain response data after individual excitation of the natural modes.

The major mechanical components are modeled with rigid bodies that are connected by different types of joints with discrete stiffness and damping. The main bodies are the rotor blades, the hub, the bodies related to the control system, the rotor mast, the nacelle, and the rigid wing beam. The main articulations are the gimbal joint represented by an ideal spherical joint, and the equivalent suspension mechanism of the wing. The secondary joints are the rotor tilt actuator, which is fixed in the airplane configuration for this study, the rotor drive articulation, a joint that prescribes the trajectory of the vehicle in space and various articulations belonging to the control system and constant velocity joint.

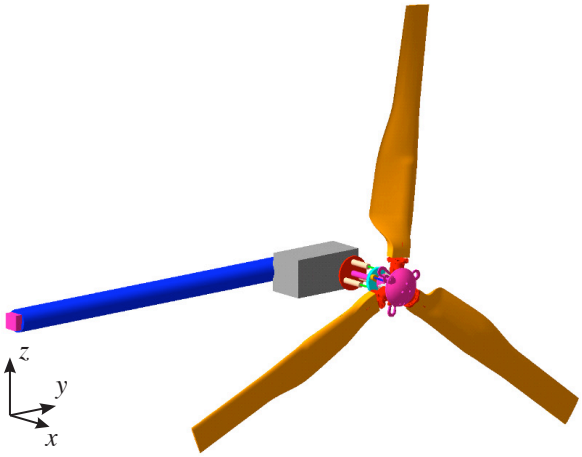

Fig. 2. Multibody model, global view.

Tabel 2. Natural frequencies of the fundamental wing modes.

Characteristic	Symbol	Frequency , Hz
beamwise bending	f_b	5.1
chordwise bending	f_c	7.2
torsion	f_t	10.5

The constant velocity joint is a V-22 like concept that is based on three flexible drive links. It is designed to transfer the mast torque to the rotor hub that inclines due to cyclic pitch. Three drive links are connected on one side to the apices of a star fixed on the mast and on the other side to the hub. As the hub side prescribes a movement out of the plane perpendicular to the mast, the drive links are subjected to periodic deformation. The periodic loads that are generated in the drive links balance each other, resulting in a homokinetic transmission of rotation from the mast plane to the hub plane.

The wing is approximated by a rigid beam whose length is two thirds of the half wingspan. This choice results, for a given wing tip deflection, in the deformation angle at the wing tip that a uniform beam would have. The wing stiffness is modeled by three angular spring-dampers at the beam articulation point. They are oriented in the beamwise, chordwise and torsion directions to represent the three fundamental natural modes of the wing. These spring-dampers also

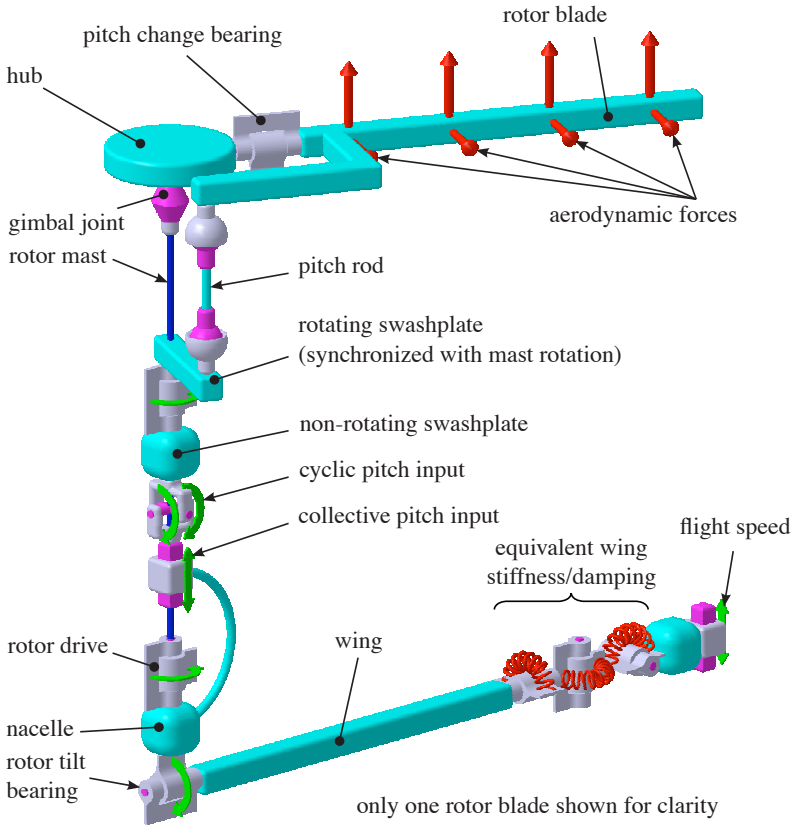

Fig. 3 . Basic kinematics of the multibody model (excluding constant velocity joint).

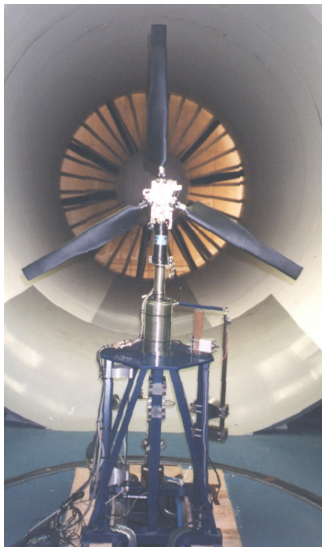

Fig. 4 . Wind tunnel model.

provide structural damping and their stiffness is chosen to yield the natural frequencies corresponding to the overall half wing assembly, including nacelle and rotor system, Table 2 . As these are structural values, they are given for the case of a non-rotating rotor with a clamped gimbal joint.

An overall view of the multibody model is given in Fig. 2 . A detailed representation of the major bodies and articulations is shown in Fig. 3 , although only one rotor blade is shown for clarity and the constant velocity joint is not represented. It should be noted that there is no individual flap or lead-lag articulation on the rotor blades. The rotation of the swashplate is synchronized with the mast by a virtual coupler.

Model Validation

An in-house aeroelastic wind tunnel model whose dynamic characteristics are adjustable to a large range of different dynamic configurations is used to determine open-loop stability behavior and to validate the numerical model. The wind tunnel model possesses a gimballed stiff-in-plane rotor and a constant velocity drive system. A picture of the model in the Eurocopter wind tunnel is given in Fig. 4 . Although the validation was made on a configuration slightly different from the ERICA Froude scaled model, it was possible to confirm the overall validity of the approach. Especially the behavior of the uncontrolled system in terms of critical speed and damping gradient has been found to be well represented after some minor adjustments of structural damping. For more detailed information, see Ref. 15 .

Control Algorithms

The study focuses on three different control algorithms: A SISO algorithm is considered first as it is a relatively simple method. Due to the nature of the algorithm, it is possible to limit its effects to a narrow frequency band and hence to reduce negative effects on the system dynamics and the pilotability of the aircraft. The present SISO algorithm is straightforward to implement as it consists of a fifth-order filter. Furthermore, its functional principle is clearly defined and the stability margins can be determined precisely, which makes it particularly suitable for industrial application. Only plant gain and phase-shift at the critical resonance frequency need to be known for the basic synthesis of the filter; however, knowledge of an analytical approximation of the eigen-mode allows a more detailed stability analysis. In the present study, a second-order transfer func-

tion is adjusted to measured gain and phase data at several discrete frequencies.

An optimal regulator with a Kalman-Bucy state estimator and Loop Transfer Recovery is the first MIMO control algorithm to be evaluated. It increases damping on more than one natural mode and therefore augments the aeroelastic stability in a more comprehensive way. This LQG/LTR algorithm is considered since the technology is well established in the industrial environment. For the synthesis of the controller, a mathematical model of the plant needs to be known. In the present study, this state-space model is obtained by system identification and the subsequent application of system realization techniques. An identification algorithm called *Autoregressive with Exogenous Input, ARX* is used in the time-domain. This method was chosen in order to evaluate its validity for the present phenomenon with the objective of applying the same algorithms to a physical wind-tunnel model. As LQG/LTR controller synthesis is performed off-line and results in a state-space model, it is easy to implement on real-time hardware for real-world experiments.

The second MIMO algorithm is Generalized Predictive Control, which has been developed more recently and is directly based on identified ARX coefficients.

Time Domain Identification

The mathematical plant model for the MIMO control algorithms is calculated from input/output time histories taken from the multibody simulations. The system identification process is based on an ARX-model of a given order p.

In discrete time, the output at time step (k) can be written as a function of the previous time steps $(k-i)$ in the following form:

$$y(k) = \sum_{i=0}^{p} \beta_i \, u(k-i) + \sum_{i=1}^{p} \alpha_i \, y(k-i) \tag{1}$$

This equation can be applied to SISO and MIMO systems, where in the latter case, the output vector y has m elements and the input vector u has r elements where m is the number of outputs and r is the number of inputs. The matrices α and β have $m \times m$ and $m \times r$ elements respectively.

When applying Eq. (1) to a sequence of l previous time steps, this yields l equations where the unknowns are the ARX coefficients α_i and β_i. A unique set of ARX coefficients can then be calculated by solving these equations in a least-squares sense. More information about the ARX model can be found in Refs. 11 and 16.

SISO Feedback

A classic approach to control vibration is the direct feedback of a measured quantity, like displacement or acceleration, to one of the control actuators. The principle of the control algorithm of this study is to calculate a command

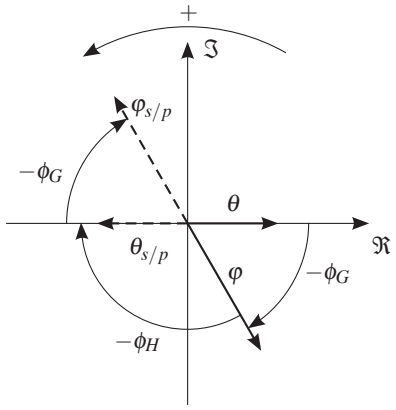

Fig. 5. Schematic of the SISO control principle. The response $\varphi_{s/p}$ acts 180° out of phase to the perturbation φ that is to be attenuated.

that generates a system response that is 180° out-of-phase with the perturbation that is to be attenuated. Phase shift and amplification are depicted in the complex plane in Fig. 5, where θ is the swashplate input and φ the plant response or output. The phase angle of this transfer function ϕ_G corresponds to the angle between the two arrows. In order to obtain a system response $\varphi_{s/p}$ which acts in opposition to a measured perturbation, the controller has to account for this phase shift. Thus, the necessary phase angle ϕ_H of the controller is:

$$\phi_H = -180^\circ - \phi_G \tag{2}$$

The mathematical formulation of the control law consists of a band-pass H_1, an all-pass H_2 and a proportional gain g. The band-pass filter reduces the disturbance of aircraft dynamics and handling characteristics by filtering out the dynamics that are not associated with the critical mode:

$$H_1 = \underbrace{\frac{s^2}{s^2 + 2\zeta_H \omega_{hp} s + \omega_{hp}^2}}_{\text{high pass}} \cdot \underbrace{\frac{\omega_{lp}^2}{s^2 + 2\zeta_H \omega_{lp} s + \omega_{lp}^2}}_{\text{low pass}} \tag{3}$$

The cut-off frequencies ω_{hp} and ω_{lp} are chosen in the vicinity of the natural frequency of the critical mode. A high damping ration ζ_H needs to be used in order to yield low phase variation with frequency and therefore good robustness margins with respect to variations in modal frequency. The adjustment of the phase shift of the filter is done with an all-pass transfer function of the following form:

$$H_2 = \frac{-\omega_d s + 1}{\omega_d s + 1} \tag{4}$$

Here, the parameter ω_d allows variation of phase shift while maintaining a constant gain. The complete filter including a static gain g is therefore:

$$H = g \cdot H_1 \cdot H_2 \tag{5}$$

A block diagram of the feedback loop is given in Fig. 6.

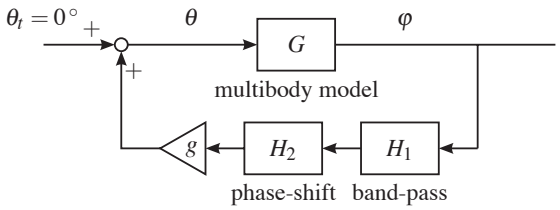

Fig. 6 . Block diagram of the SISO feedback loop.

Optimal Control

A well proven algorithm for MIMO control is the Linear Quadratic Regulator. It consists of calculating the optimal gain matrix for feedback of the system states to the plant inputs. If applied alone, the Quadratic Regulator possesses excellent performance and robustness characteristics but it is rather impractical to measure all system states. Therefore, the Quadratic Regulator is often accompanied by a Kalman-Bucy filter that estimates the states of the system on the basis of a few output measures. The so-formed Linear Quadratic Gaussian Control is the first MIMO control algorithm of this work.

Basic Problem. The starting point for the development of the Linear Quadratic Gaussian State Feedback Regulator is the linear time-invariant state-space model with noise on the system states and the output measures:

$$\begin{aligned} \dot{x} &= Ax + Bu + Mw \\ y &= Cx + v \end{aligned} \tag{6}$$

In this equation, x is the state vector, u the input vector, y the output vector, A the system matrix, B the input gain matrix, C the output gain matrix, and M is a constant matrix that is weighting the disturbances. The process noise vector w and the measurement noise vector v are non-correlated white noise with zero means and the constant, symmetric covariance matrices W (positive semi-definite) and V (positive definite) that are defined as follows:

$$\begin{aligned} \mathrm{E}\left[w(t)w(\tau)^{\mathrm{t}}\right] &= W\delta(t-\tau) \\ \mathrm{E}\left[v(t)v(\tau)^{\mathrm{t}}\right] &= V\delta(t-\tau) \\ \mathrm{E}\left[w(t)v(\tau)^{\mathrm{t}}\right] &= 0 \end{aligned} \tag{7}$$

Here, E denotes the error function, δ the Dirac or delta function, and $^{\mathrm{t}}$ the transpose.

The LQG synthesis consists of finding a control law that stabilizes the system and minimizes the quadratic performance index

$$J = \lim_{T\to\infty} \mathrm{E}\left[\int_0^T \left(x^{\mathrm{t}}Qx + u^{\mathrm{t}}Ru\right)\mathrm{d}t\right] \tag{8}$$

where Q is a constant, symmetric and positive semi-definite matrix and R is constant, symmetric and positive definite. These weighting matrices give the relative importance of state distortion and control power. It is useful to set $Q = C^{\mathrm{t}}C$ which allows the distortions to be weighted in terms of the physical output measurements. In the present study, the inputs as well as the output measurements are angles of the same order of magnitude. The weighting matrix R is therefore set to the identity matrix I, which gives an equal importance to output distortion angles and command angles.

State Estimator, Kalman-Bucy filter. The first step of the synthesis of an LQG controller is to search for the maximum likelihood / minimum variance estimate $\hat{x}$ of the state vector.

The state estimator dynamics is given by

$$\dot{\hat{x}} = A\hat{x} + Bu + K_f(y - C\hat{x}) \tag{9}$$

where the estimation error $y - C\hat{x}$ needs to tend to zero asymptotically.

The optimal estimator (or Kalman) gain matrix is $K_f = P_f C^{\mathrm{t}} V^{-1}$ where P_f is the constant, symmetric, positive definite solution of the following algebraic matrix Riccati equation:

$$P_f A^{\mathrm{t}} + AP_f - P_f C^{\mathrm{t}} V^{-1} C P_f + MWM^{\mathrm{t}} = 0 \tag{10}$$

Here, $W_x = MWM^{\mathrm{t}}$ can be interpreted as the covariance matrix of the state noise that can expressed in terms of the more physical input noise by setting $W_x = BB^{\mathrm{t}}$. The covariance of the measurement noise is taken to be equal for all angle measurements and can therefore be set to $V = \rho I$ with the parameter ρ for adjusting the convergence speed of the estimator dynamics.

Linear Quadratic Gaussian Regulator. By using the estimated state vector, a linear quadratic regulator can now be designed. It consists of finding a gain matrix K_c so that the feedback $u(t) = -K_c\hat{x}(t)$ stabilizes the system and minimizes the quadratic performance index Eq. (8).

This optimal controller gain is given by

$$K_c = R^{-1}B^{\mathrm{t}}P_c \tag{11}$$

where P_c is the constant, symmetric, positive definite matrix solution of the algebraic Riccati equation:

$$P_c A + A^{\mathrm{t}}P_c - P_c B R^{-1} B^{\mathrm{t}} P_c + Q = 0 \tag{12}$$

Loop Transfer Recovery. The LQR and the Kalman-Bucy filter have excellent individual robustness characteristics. However, when used in combination, the resulting LQG has much smaller stability margins. The objective of *Loop Transfer Recovery, LTR* is to chose the matrices W_x and V appropriately in order to recover asymptotically the robustness of either the LQR or the Kalman-Bucy filter. Therefore, the stochastic nature of the process environment modeling is discarded in favor of robustness and performance criteria.

The objective is to recover the open-loop transfer function of the LQR $-K_c\left(sI - A\right)^{-1}B$ via the open-loop transfer function $K(s)\cdot G(s)$ of the LQG regulator. In the present case

and under the hypothesis of a minimum phase transfer function G, this can be achieved when the factor ρ tends to zero. On the other hand, it is important not to choose too small a value for ρ in order to avoid very fast estimator dynamics. An overly fast estimator would degrade the complementary output sensitivity function at high frequency and therefore reduce robustness to non-structured uncertainty.

Generalized Predictive Control

GPC is a receding-horizon LQ control law for which the future control sequence is recalculated at each time step. The method used in the present work is based on the ARX model as described in Ref. 17 .

A key feature of GPC is the calculation of control action according to the predicted reaction of the system. Thus, the algorithm allows the choice of the controller speed in a wide range between the extreme deadbeat (minimum-time) behavior with high control effort, and an approximation of the minimum control energy solution.

Multi-Step Output Prediction. The ARX equation Eq. (1) can be interpreted as a one-step prediction of system response y into the future:

$$y(k) = \beta_0^{(0)}\, u(k) + \sum_{i=1}^{p} \beta_i^{(0)}\, u(k-i) + \sum_{i=1}^{p} \alpha_i^{(0)}\, y(k-i) \quad (13)$$

Here the superscript $^{(0)}$ denotes the current time step.

When recursively applying this equation for successive prediction time steps, the predicted output at time step j in the future can be written as follows:

$$\begin{aligned} y(k+j) = &\sum_{i=0}^{j} \beta_0^{(i)} u(k+j-i) \\ &+ \sum_{i=1}^{p} \beta_i^{(j)} u(k-i) + \sum_{i=1}^{p} \alpha_i^{(j)} y(k-i) \end{aligned} \quad (14)$$

where all ARX coefficients beyond the model order are assumed to be equal to zero. The remaining coefficients $\alpha_i^{(j)}$ and $\beta_i^{(j)}$ are calculated in a recursive manner according to:

$$\begin{aligned} \beta_i^{(j)} &= \beta_{i+1}^{(j-1)} + \alpha_1^{(j-1)} \beta_i^{(0)} \\ \alpha_i^{(j)} &= \alpha_{i+1}^{(j-1)} + \alpha_1^{(j-1)} \alpha_i^{(0)} \end{aligned} \quad (15)$$

In these equations, the coefficients at $j = 0$, $\alpha_i^{(0)}$ and $\beta_i^{(0)}$, are the observer Markov parameters α_i and β_i which have been identified by means of the ARX model, Eq. (1).

When grouping the future inputs and outputs according to

$$u_{h_c} = \begin{bmatrix} u(k) \\ u(k+1) \\ \vdots \\ u(k+h_c-1) \end{bmatrix}, \quad y_{h_p} = \begin{bmatrix} y(k) \\ y(k+1) \\ \vdots \\ y(k+h_p-1) \end{bmatrix} \quad (16)$$

and the past inputs and outputs according to

$$u_p = \begin{bmatrix} u(k-1) \\ u(k-2) \\ \vdots \\ u(k-p) \end{bmatrix}, \qquad y_p = \begin{bmatrix} y(k-1) \\ y(k-2) \\ \vdots \\ y(k-p) \end{bmatrix} \quad (17)$$

the multi-step output prediction equation Eq. (14) can be put into matrix form:

$$y_{h_p} = T_p\, u_{h_c} + B_p\, u_p + A_p\, y_p \quad (18)$$

with the matrices A_p, B_p and T_p being composed of the coefficients $\alpha_j^{(i)}$ and $\beta_j^{(i)}$ according to Eq. (14) and Eq. (15). Here, the future inputs and outputs are assumed to be zero beyond the respective control horizon h_c and prediction horizon h_p where $h_c \leq h_p$. The matrices are therefore known at each time step and the only unknowns are the future outputs y_{h_p} as functions of the future inputs u_{h_c}.

Control Law. The objective of the GPC algorithm is to calculate the future inputs in order to achieve the desired output. The regulation error can therefore be formulated using Eq. (18) as the difference of system response y_{h_p} from the target response y_t:

$$\varepsilon = y_t - y_{h_p} = y_t - T_p\, u_{h_c} - B_p\, u_p - A_p\, y_p \quad (19)$$

For the present regulator problem, the target response y_t is equal to zero.

A cost function that is quadratic in the error as well as in the future control inputs can be formulated similar to the LQR problem of Eq. (8):

$$J = \varepsilon^{\mathrm{t}} Q \varepsilon + u_{h_c}^{\mathrm{t}} R u_{h_c} \quad (20)$$

The weighting matrix Q is constant, symmetric and positive semi-definite and R is constant, symmetric and positive definite. Similar observations as in the LQR problem suggest diagonal matrices with equal coefficients for the r control inputs and the m system outputs. Here the matrices are set to $Q = I$ and $R = w_r I$ with the parameter w_r to be tuned during closed-loop simulations.

Minimizing J with respect to u_{h_c} and solving for this vector yields

$$u_{h_c} = -\left(T_p^{\mathrm{t}}\, Q\, T_p + R\right)^{\dagger} T_p^{\mathrm{t}}\, Q\, \left(-y_T + B_p\, u_p + A_p\, y_p\right) \quad (21)$$

which gives the future control input up to the control horizon. Only the first time step is used as control input at the present time step and a new control sequence is calculated at the next time step. The pseudo-inverse $()^{\dagger}$ gives the solution in a least-squares sense and is computed using singular value decomposition.

Choice of the Controller Parameters. The ARX model order p can be considered as the speed of the implicit observer. It is to be chosen so that $p \cdot m \geq n$ where n is the assumed number of significant natural modes and m the number of outputs. This only holds if disturbance states are not to be accounted for.

The speed of the implicit controller is governed by the prediction horizon h_p that needs to be greater than or equal to p. Higher values move the controller away from the deadbeat solution towards a low control energy solution. Here, the prediction horizon is set equal to the model order and the control energy is adjusted using the weighting matrices in the cost function J. The control horizon h_c needs to be less than or equal to the prediction horizon h_p; for this study $h_c = h_p$.

SIMULATION PARAMETERS

Simulation Procedure

The simulations are carried out in the time domain and can be divided into three phases: First, the aircraft is accelerated to its cruise speed, starting with rotor and aircraft at rest. During this phase, the rotor is driven by the aerodynamic forces and the collective blade pitch is set by a Proportional-Integral (PI) feedback controller in order to adjust the rotor nominal rotation speed. This feedback loop is deactivated as soon as a steady flight condition is reached to avoid any disturbance of the stability measurements. During the acceleration phase, the wing is clamped by means of high spring stiffnesses. Once the nominal flight speed is reached, the wing clamp is removed and the controller is activated. In order to allow the rotor to reach a steady flight condition, several rotor revolutions are simulated without any external disturbances. Next, the model is excited by adequate swashplate input at the frequency of the mode of interest, and the time history is recorded. The free decay response of the oscillations is analyzed using Fast Fourier Transforms and a moving block method in order to extract modal frequency and normalized damping.

The sampling frequency of the simulations is set to 200 Hz ($\approx {}^{12.6}/_{\text{rev}}$) in order to have a reasonable number of time steps per rotor revolution. This choice also provides a good resolution of the natural modes (frequencies up to 35 Hz have been found), which are well beneath the Nyquist frequency.

Controller action is calculated on-line with dedicated control software. Data exchange between the dynamics simulation and the controller is done for a number of measured values of plant inputs and outputs at each simulation time step. The main plant outputs are the three wing degrees of freedom, the gimbal flapping angles and rotor rpm. On the input side, there are mainly three swashplate actuator commands that are calculated from the input commands θ_0, θ_{1c} and θ_{1s}.

ARX Identification

For system identification, the plant model needs to be excited by a signal with a large frequency content. In this study, the excitation signal is white noise that is band-pass filtered between 1 Hz and 75 Hz. This choice is mainly for practical reasons as white noise can be easily generated during the subsequent wind tunnel tests.

In the present work, the system is identified once and the controllers are synthesized off-line based on this data. This is done for a number of advance ratios at equal increments of 0.14 up to $= 0.83$, which is just beneath the uncontrolled stability limit. During closed-loop simulations, the controller corresponding to the current aircraft speed is applied up to $= 0.83$. Above this advance ratio, the same controller is maintained. The controller parameters are optimized at $= 0.83$ and the same parameters are used in the entire velocity range.

The major parameters of the identification algorithm are model order and length of the identification time histories. For both MIMO control applications, a number of $l = 1000$ time steps is taken into account which covers about 20 periods of the lowest natural frequency. The state-space models of the LQG synthesis are identified at an order of $p = 10$ whereas the GPC controller is designed with a lower order of $p = 5$.

Controller Parameters

SISO Control Parameters. The primary design objective of the controllers is to augment the aeroelastic stability of the aircraft. Basically, only one axis can be stabilized with the present SISO controller and it is therefore designed to augment the damping of the first mode to go unstable. Here, this is the wing beamwise bending mode q_b. Therefore the displacement measurement φ_b of the associated degree of freedom is taken as plant output. The analysis of the dynamics of the uncontrolled system indicated a high-gain transfer function between the longitudinal cyclic input θ_{1c} and φ_b which leads to the choice of θ_{1c} as input command.

The resonance frequency at $= 0.83$ is situated at 4.6 Hz and plant phase shift is about $\phi_G|_{4.6\,\text{Hz}} = -60\,^\circ$. The optimal controller phase shift would therefore be $\phi_H|_{4.6\,\text{Hz}} = -120\,^\circ$. During the studies it was found that the plant resonance frequency decreases slightly with increasing flight speed. Consequently, the phase angle of the controller decreases and the optimal phase shift is no longer provided. In order to compensate for this phenomenon and therefore have a more robust design, a slightly higher filter phasing of $\phi_H|_{4.6\,\text{Hz}} = -150\,^\circ$ is chosen. This is a good compromise between maximum damping at the design speed and good robustness at higher flight speed. Furthermore, the cut-off frequencies ω_{hp} and ω_{lp} of the band-pass filter Eq. (3) are chosen at about ± 0.5 Hz of the dominating natural frequency, and the damping ratio is set to $\zeta_H \approx 0.7$. In order to optimize the controller gain g with respect to system damping,

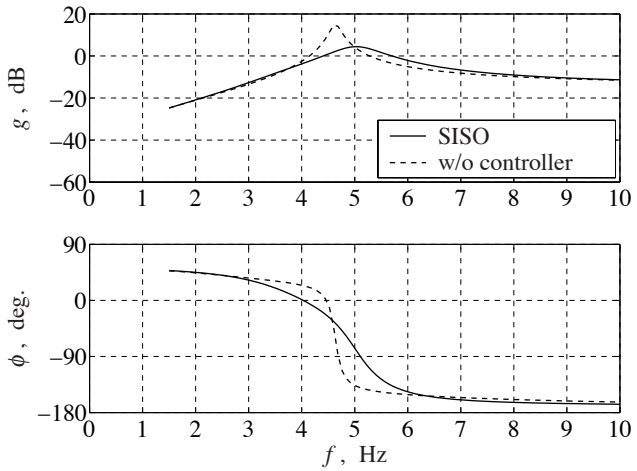

Fig. 7 . Transfer function from θ_{1c} to φ_b with and without SISO controller.

standard root-locus techniques have been applied. This results in an optimal gain close to $g = 1$. For this filter, the slope of the phase angle curve at the resonance frequency is $-4.1\,{}^{\text{deg.}}/_{0.1\text{Hz}}$ which is sufficient for good parameter robustness.

A Bode diagram of the closed-loop behavior in comparison to the uncontrolled system is given in Fig. 7 . The associated gain and phase margins are 12 dB and 59°, which is a reasonable trade-off between bandwidth and stability.

Optimal Control Parameters. In this study, the main concern is the aeroelastic stability of the wing modes which have low damping. The three degrees of freedom to be stabilized are wing beamwise bending, wing chordwise bending and wing torsion. Therefore, the corresponding angles φ_b, φ_c, and φ_t are taken as plant output. When analyzing plant dynamics, it turns out that all three swashplate inputs have a large influence on the plant outputs, albeit there are privileged transfers of high gain as for example the transfers θ_{1c} to φ_b, θ_{1c} to φ_t and θ_0 to φ_c. All three plant inputs are therefore controlled.

As described above, the main parameter of the optimal controller is the weighting factor ρ, which determines the relative covariance of the measurement noise with respect to the state noise. A value of $\rho = 10^{-4}$ is appropriate as the open-loop singular values of the LQG well recover the singular values of the open-loop LQR in a frequency range between approximately 1 Hz and 30 Hz, which encloses the three main natural modes. The chosen value resulted in considerable damping augmentation on the modes and good robustness with respect to flight speed.

Generalized Predictive Control Parameters. The main parameters of the GPC controller are the model order, the prediction and control horizons and the weighting parameter w_r. There are five significant natural modes in the plant model, and the three plant outputs. An order of $p = 5$ is therefore sufficient when there is no need to take into account any disturbance states. In this case, a rather quick controller can be designed which results in a choice of the prediction and control horizons of $h_c = h_p = 5$. Under these conditions, the weighting factor for good system damping with adequate control energy is $w_r = 0.1$. The plant inputs and outputs have been chosen identical to LQG control.

RESULTS

Controller Performance

The performance of all three controllers with respect to damping augmentation is shown in Fig. 8 . Here, the eigenvalues of the principal modes are shown as a function of in the complex plane. The progressive gimbal mode β_+ is not much affected by the controller and as its eigenvalue is higher than those of the other modes, it is not shown in the graphs. Each sub-figure includes the principal natural modes of the uncontrolled system for reference. The critical advance ratio of the uncontrolled system is $= 0.94$. As the regressive gimbal mode β_- of the uncontrolled system has very high damping, it does not appear on the charts.

All three controllers considerably augment stability and only slightly influence model frequencies. Flutter speed is $_{crit} = 1.11$ for SISO control, $_{crit} = 1.21$ for LQG and $_{crit} = 1.15$ for GPC, which constitutes an increase of 18 %, 29 % and 22 % respectively. In either case it is the β_- mode that goes unstable first – see also Ref. 10 for a similar behavior. As this mode is not considered in the controller design, the critical speed is largely independent of the controller type but the overall better performance of the MIMO controllers is also favorable to this mode. The results give sufficient perspectives for practical applications as they show considerable stability augmentation up to the flutter speed of the uncontrolled system and slightly beyond. Therefore, stabilization of the β_- mode has not been considered in this work.

The SISO controller, Fig. 8 **a.)** , considerably stabilizes the most critical q_b mode: Near the natural flutter speed, the damping ratio rises to about 10 % and exhibits a positive gradient. Furthermore, a slight stabilization of the q_t mode can be observed while there is almost no impact on the q_c mode. Generally, there is little effect on damping at low speed, which was expected as the controller is tuned at $= 0.83$.

Concerning the LQG controller it is noted from Fig. 8 **b.)** that the achieved damping on the q_b mode is about twice the value obtained with the SISO controller. In addition, the q_c mode is increasing its damping to 12 % at the uncontrolled flutter speed whereas, comparable to the SISO case, the torsion mode is not much affected.

The GPC controller, Fig. 8 **c.)** , achieves slightly better results on the q_b mode than LQG and is the only controller that considerably augments the damping of the q_t mode.

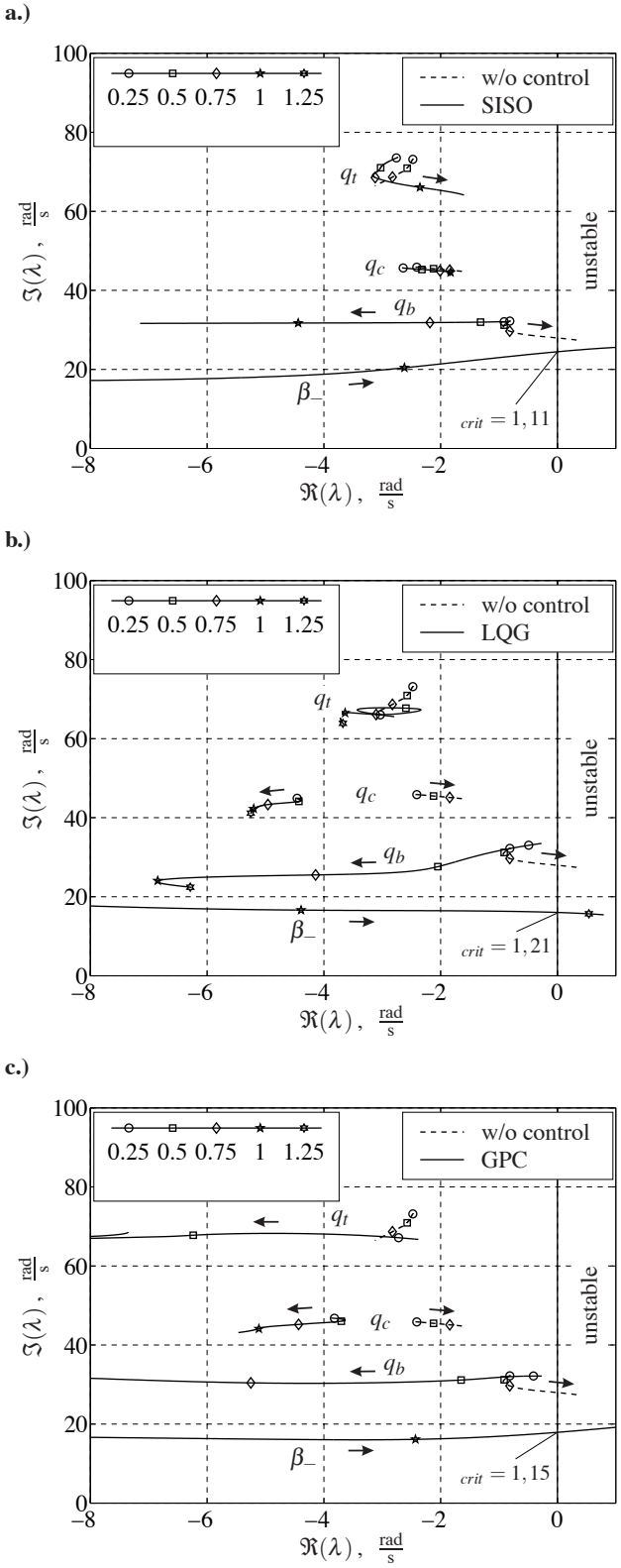

Fig. 8. Root loci of the main natural modes as a function of advance ratio : a.) SISO control, b.) LQG, c.) GPC.

However, this occurs at the expense of the β_- mode which yields a lower flutter speed compared to the LQG controller. Results on the other modes are only slightly different from

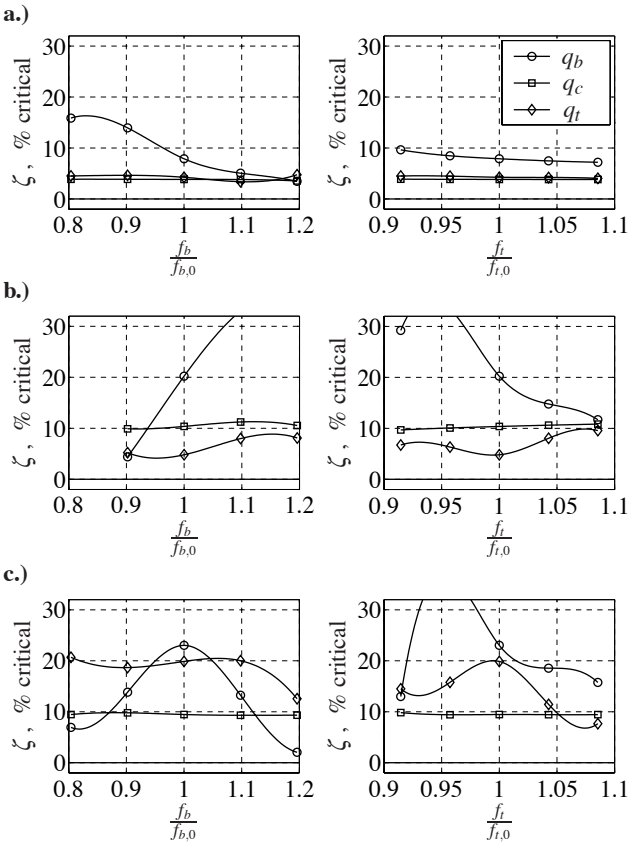

Fig. 9. Robustness of the controllers at = 0.83: a.) SISO control, b.) LQG, c.) GPC.

LQG control.

Robustness

Robustness of the controllers is analyzed with respect to variations in beamwise bending (f_b), chordwise bending (f_c) and torsion (f_t) natural frequencies. The influence of simultaneous changes in structural damping (ζ_s) of all wing modes, rotor rotational frequency (Ω), altitude (h) and white measurement noise is also assessed. The results for f_b and f_t are presented in Fig. 9 **a.)** to **c.)** for the three controllers. The baseline value of each parameter is denoted by the index zero.

In closed-loop, the wing beamwise bending mode experiences the highest damping augmentation. Variations of its natural frequency (f_b) considerably influence the controller performance with regard to this mode. The SISO controller yields a higher stability gain at lower frequencies f_b whereas LQG performs better at high frequencies. GPC control is degrading for either deviation from the nominal value. Modifications of the torsion frequency tend to decrease beamwise damping at higher frequency, but very low frequencies also degrade the behavior of both MIMO controllers. The impact on other modes is quite small.

It has also been observed that structural damping has little influence on the stability gain due to SISO and LQG,

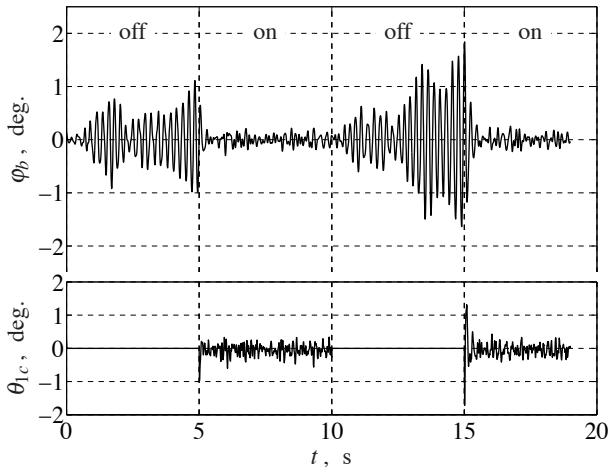

Fig. 10 . Efficiency of LQG controller and control effort, wing beamwise bending mode, $= 0.97$.

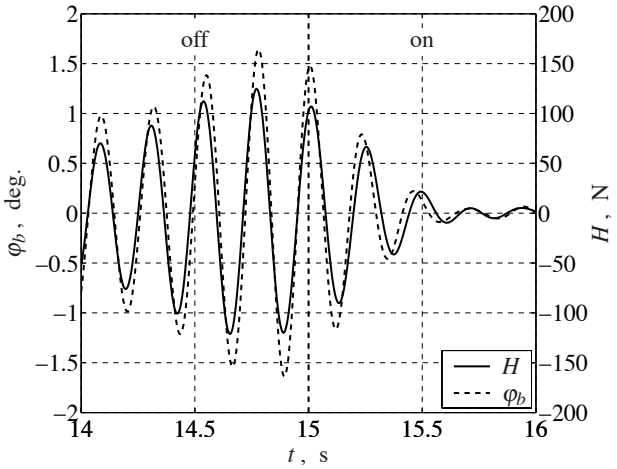

Fig. 11 . H-force acting on the q_b mode, $= 0.97$.

and it only has a small effect on GPC. Furthermore, aerodynamic damping as well as controller generated shear forces decrease with flight altitude h. This leads to a decrease in overall damping but there is no negative effect on controller performance. Corresponding graphs of the robustness with respect to structural damping and flight altitude are therefore not given here.

The rotor rotation speed did not have a notable influence on controller behavior. Variations in chordwise bending frequency also have very limited influence on the three controllers as the associated natural mode is almost decoupled from the other natural modes. The SISO and the LQG controllers were very robust with respect to measurement noise; only GPC was not able to handle noisy measurement signals. In the latter case, a noise level of 5 % of the maximum wing deformation angle destabilized the controller. In general, all three controllers performed quite well for simultaneous variations of the parameters.

Control Power, Flutter Mechanism

In the current study, the controller commands are transmitted to the rotor via the swashplate. The command angles are therefore a measure for the control effort. Figure 10 gives a simulation time history with LQG controller in the loop for an advance ratio of $= 0.97$ that is slightly above the natural stability limit but stable in closed-loop. For this simulation, the model is excited by white noise of an amplitude of about 0.5° on the collective and 1° on the cyclic inputs. The main swashplate input θ_{1c} is also represented and it can be seen that only moderate input commands of well below 1° are necessary. The amplitudes on the other inputs are even smaller. However, the abrupt activation of the controller resulted in a control command with a high bandwidth and an amplitude of about 1.9°.

Figure 11 shows an enlargement of the wing deformation measure from Fig. 10 and the corresponding rotor longitudinal H-force in the vicinity of $t = 15$ s when the controller is turned on. Both signals are zero-phase band-pass filtered between 3 Hz and 5.5 Hz. The H-force presented in the graph is oriented vertically in the airplane configuration and acts directly on the q_b and the q_t mode. It is seen to have a slight phase lead with respect to the wing deformation φ_b. By this mechanism, the rotor aerodynamic force is injecting energy into the wing mode that can ultimately drive the system unstable. Starting from $t = 15$ s the controller is turned on and the phase lead of the H-force is transformed into a phase lag which is stabilizing.

CONCLUSIONS

This work presents the development and the evaluation of three different controllers designed to augment whirl flutter stability of tiltrotor aircraft in high speed level flight. A simulation model of the wing/pylon/rotor system was set up using a general purpose multibody simulation tool. Time domain simulations were performed with a controller in the loop. The primary conclusions are:

1) SISO control yields 17 % increase in flutter speed whereas GPC achieves 21 % and LQG almost 29 % .

2) At high flight speeds, the regressive gimbal mode becomes unstable while the wing modes are well damped.

3) The most critical natural mode, the beamwise bending mode, is well stabilized by all controllers. In addition, the damping of the chordwise bending mode is increased by both MIMO controllers and the damping of the torsion mode only by GPC.

4) In a steady flight condition, low control effort of considerably less than 1° of swashplate angle is necessary to stabilize the system.

5) The controllers are generally very robust with respect to variations of natural frequency, structural damping, flight

altitude, rotor rotation speed, measurement noise and flight speed. However, a wing bending natural frequency well bellow 90 % of the nominal value can destabilize the LQG/LTR control loop. Furthermore, the GPC is less tolerant to variations in wing torsion frequency and it has very low robustness with respect to noisy measurement signals.

6) The controllers stabilize the wing beamwise bending mode by generating rotor in-plane forces of adequate magnitude and phase angle.

From this study it can be concluded that the LQG/LTR algorithm is the most promising for subsequent wind tunnel tests. It shows good performance and robustness characteristics when an identified plant model can be provided. Especially its good robustness with respect to measurement noise gives it an advantage over the GPC controller. For industrial application, the SISO controller may be more appropriate as its dynamics are well defined and its influence on aircraft behavior can be precisely predicted.

ACKNOWLEDGEMENTS

The work presented in this paper has been co-funded by a Marie Curie Scholarship (5th Research Framework Program of the European Commission) and Eurocopter, Marignane, France. It was partially carried out at ENSICA, Toulouse, France. The contributions of ENSICA and Eurocopter staff are largely acknowledged.

REFERENCES

[1] Hall, W. E., Jr.: Prop-Rotor Stability at High Advance Ratios. *Journal of the American Helicopter Society*, 11(3):11–26. June 1966.

[2] Nixon, M.: Parametric Studies for Tiltrotor Aeroelastic Stability in Highspeed Flight. *Journal of the American Helicopter Society*, 38(4):71–79. October 1993.

[3] Hathaway, E. L. and Gandhi, F. S.: Design Optimization for Improved Tiltrotor Whirl Flutter Stability. In *29th European Rotorcraft Forum*. Friedrichshafen, Germany. September 16-18, 2003.

[4] Ghiringhelli, G. L.; Masarati, P.; Mantegazza, P. and Nixon, M. W.: Multi-Body Analysis of an Active Control for a Tiltrotor. In *CEAS Intl. Forum on Aeroelasticity and Structural Dynamics*, pp. 149–158. Williamsburg, Virgina. June 22–25, 1999.

[5] Manimala, B.; Padfield, G. D.; Walker, D.; Naddei, M.; Verde, L.; Ciniglio, U.; Rollet, P. and Sandri, F.: Load Alleviation in Tilt Rotor Aircraft through Active Control; Modelling and Control Concepts. In *American Helicopter Society, 59th Annual Forum*. Phoenix, Arizona. May 6–8, 2003.

[6] Komatsuzaki, T.: *An Analytical Study of Tilt Proprotor Aircraft Dynamics in Airplane Cruise Configuration Including the Effects of Fuselage Longitudinal Rigid Body Motion*. Ph.D. thesis, Princeton University. January 1980.

[7] Nasu, K.: *Tilt-Rotor Flutter Control in Cruise Flight*. TM 88315, NASA. December 1986.

[8] van Aken, J. M.: Alleviation of Whirl-Flutter on Tilt-Rotor Aircraft using Active Controls. In *American Helicopter Society, 47th Annual Forum*. Phoenix, Arizona. May 6–8, 1991.

[9] Vorwald, J. G. and Chopra, I.: Stabilizing Pylon Whirl Flutter on a Tilt-Rotor Aircraft. In *32nd AIAA/ASME/ASCE/AHS/ASC Structures, Structural Dynamics, and Materials Conference*. Baltimore, Maryland. April 8–10, 1991. Article AIAA-91-1259-CP.

[10] Wang, J. C.: A Tilt-Rotor Aircraft Whirl-Flutter Alleviation Using Active Controls. In J. Clark et al., eds., *Active control of noise and vibration.*, vol. 38, pp. 139–148. American Society of Mechanical Engineers, New York. 1992.

[11] Kvaternik, R. G.; Piatak, D. J.; Nixon, M. W.; Langston, C. W.; Singleton, J. D.; Bennett, R. L. and Brown, R. K.: An Experimental Evaluation of Generalized Predictive Control for Tiltrotor Aeroelastic Stability Augmentation in Airplane Mode of Flight. *Journal of the American Helicopter Society*, 47(3):198–208. July 2002.

[12] Nixon, M.; Langston, C.; Singleton, J.; Piatak, D.; Kvaternik, R.; Corso, L. and Brown, R.: Aeroelastic Stability of a Four-Bladed Semi-Articulated Soft-Inplane Tiltrotor Model. In *American Helicopter Society, 59th Annual Forum*. Phoenix, Arizona. May 6–8, 2003.

[13] Hathaway, E. L. and Gandhi, F. S.: Modeling Refinements in Simple Tiltrotor Whirl Flutter Analyses. *Journal of the American Helicopter Society*, 48(3):186–198. July 2003.

[14] Nannoni, F.; Giancamilli, G. and Cicalè, M.: ERICA: The European Advanced Tiltrotor. In *27th European Rotorcraft Forum*. Moscow, Russia. September 11–14, 2001.

[15] Mueller, J. P.: *Méthodologie d'Optimisation Aéroélastique Active d'une Voilure de Convertible – Flottement Gyroscopique*. Ph.D. thesis, Université Paul Sabatier (Toulouse III), Toulouse, France. October 2004.

[16] Juang, J.-N.: *Applied System Identification*. PTR Prentice-Hall, Englewood Cliffs, New Jersey. 1994.

[17] Phan, M. Q. and Juang, J.-N.: Predictive Controllers for Feedback Stabilization. *Journal of Guidance, Control, and Dynamics*, 21(5):747–753. September–October 1998.